Mirror Symmetry Broken of Sound Vortex Transmission in a Single Passive Metasurface via Phase Coupling

Yugan Tang,[1] Boyang Xie,[1] Hui Liu,[1] Ya Zhang,[1] Hua Cheng,[1,*] and Shuqi Chen[1,2,3,†]
[1]The Key Laboratory of Weak Light Nonlinear Photonics, Ministry of Education, School of Physics and TEDA Institute of Applied Physics, Nankai University, Tianjin 300071, China
[2]School of Materials Science and Engineering, Smart Sensing Interdisciplinary Science Center, Nankai University, Tianjin 300350, China
[3]The collaborative Innovation Center of Extreme Optics, Shanxi University, Taiyuan, Shanxi 030006, China

(Received 9 October 2023; accepted 29 March 2024; published 23 April 2024)

Asymmetric transmission in a passive vortex system is highly desirable, as it enables the development of compact vortex-based devices. However, breaking the mirror symmetry of transmission via a single metasurface poses challenges due to the inherent symmetric transmission properties in reciprocity. Here, we theoretically propose and experimentally demonstrate a novel transmission-reflection phase coupling mechanism to achieve the broken mirror symmetry of sound vortex transmission. This mechanism establishes a special coupling link between transmission and reflection waves, superimposing asymmetric reflection phases on the transmission phases. By utilizing a single passive phase gradient metasurface with asymmetric reflection phase twists, distinct transmission phase twists for mirror-symmetric incident vortices can be achieved within a cylindrical waveguide. This is typically difficult to implement in a reciprocal system. Numerical and experimental results both demonstrate the broken mirror symmetry of vortex transmission and reflection. Our findings offer a new strategy for controlling vortex wave propagation, which may inspire new directional applications and extend to the field of photonics.

DOI: 10.1103/PhysRevLett.132.177001

The development of metasurfaces has sparked a growing interest in exploring complex fields with a higher degree of freedom [1,2]. One such field is the vortex field that carries orbital angular momentum (OAM), which offers orthogonal modes and can be passively generated using the spiral phase of a phase gradient metasurface (PGM) [3–6]. Because of the excellent prospects of OAM-based applications in acoustic and optical communication [6–9], particle manipulation [10], and torque [11], achieving asymmetric effects with space-efficient design holds great potential for directional applications. In contrast to nonreciprocal modulations that require active devices or bulky configurations with external intervention, reciprocal modulations employing passive and simple structures offer greater flexibility and suitability for compact systems. However, the symmetric scattering matrix of a reciprocal system makes it difficult to realize asymmetric transmission phases. The electromagnetic waves can obtain asymmetric transmission phases through polarization conversion and composite layer stacking [12,13], while the acoustic waves are generally regarded as scalar pressure fields that lack such degrees of freedom. Thus, breaking the symmetric transmission effects on a single passive metasurface remains an intriguing question in acoustics.

Recent advancements have revealed that multiple internal reflections (MIRs) provide a new paradigm to manipulate transmission and reflection wave fields via diffraction [14–20]. This mechanism enables an external phase accumulation that depends on the propagation number. The acoustic vortex diffraction law, which benefits from MIRs, has been presented [18]. By utilizing a single PGM, it allows asymmetric transmission for opposite incident vortices with same topological charges. Moreover, asymmetric vortex transmission for opposite plane wave incidences can be achieved by combining two PGMs [19]. However, the unit cells of the PGM in previous works still exhibit symmetric transmission phases owing to reciprocity [3–6,18,19]. Consequently, the transmission phase twists generated by a single PGM are essentially definite, which can create a mirror-symmetric effect on the equivalent incident waves originating from opposite directions. If the backward incident vortex irradiated onto the PGM adopts equivalent cases (mirror-symmetric) with the forward one, then the corresponding transmitted vortex will also exhibit mirror symmetry (Supplemental Material, Sec. A [21]). Therefore, proposing a new physical mechanism to break the mirror symmetry of vortex transmission with a single PGM would be highly valuable.

In this Letter, inspired by the acoustic vortex diffraction law, we theoretically present and experimentally validate for the first time a transmission-reflection phase coupling (TRPC) mechanism. This mechanism breaks the mirror

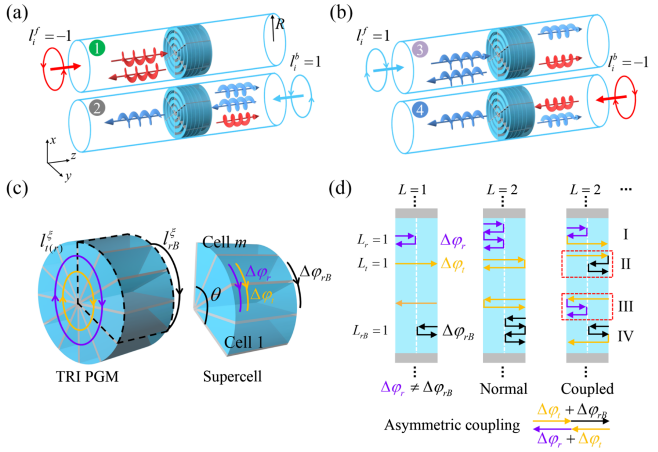

FIG. 1. Schematic of asymmetric generation and propagation of mirror-symmetric incident vortices. (a), (b) Transmission and reflection of mirror-symmetric vortex in a cylindrical waveguide. Red and blue spirals represent vortices with topological charges of −1 and 1, respectively. (c) Schematic diagram of a single TRI PGM, which is composed of groups of fanlike supercells. (d) Illustration of MIRs effect with normal and coupled processes in a 2D cross section of the unit cell for forward and backward incidences.

symmetry of vortex transmission within a cylindrical waveguide by employing a single transmission-reflection-integrated (TRI) PGM. Generally, a single PGM employs only transmission or reflection response of unit cells, serving primarily to introduce fixed phase twists without achieving substantial change in mirror-symmetric transmission properties. The introduced TRI PGM possesses both transmission and reflection responses enabling TRPC during MIRs, thereby superimposing the reflection phases on the transmission phases. Remarkably, the mechanism of transmission phase control and the structural design method are fundamentally different from previous studies. Empowered by TRPC, the designed TRI PGM enables asymmetric transmission for mirror-symmetric incident vortices. Figure 1(a) shows the one-way transmission, and Fig. 1(b) shows the asymmetric transmission with different topological charges. The superscripts f and b indicate the directions of forward and backward propagation, respectively, and subscript i represents the incidence. The generalizable mechanism presented herein offers a distinctive platform for generating asymmetric vortices and efficiently shifts the paradigm in compact acoustic devices.

To reveal this unusual mechanism, we commence by introducing a TRI PGM structure arranged in a rigid cylindrical waveguide of radius R, as shown in Fig. 1(c). Each unit cell can be regarded as an equivalent medium separated by thin sound-hard plates [see the gray regions in Fig. 1(c)]. By discretizing the phases of fanlike unit cells to provide phase gradients in azimuth, the phase twists are achieved. Since the unit cell designed here uniquely supports both transmission and reflection phase modulations [23], waves incident on the unit cell will not only transmit, but also be reflected. The corresponding transmission and reflection phase shifts will be further obtained. M fanlike unit cells are divided into $|l^{\xi}_{t(tB)}|$ and $|l^{\xi}_{r(rB)}|$ groups of fanlike supercells, each with an angular width of $\theta_{t(tB)} = 2\pi/|l^{\xi}_{t(tB)}|$ and $\theta_{r(rB)} = 2\pi/|l^{\xi}_{r(rB)}|$, respectively. This division enables simultaneous provision of transmission and reflection phase twists, where subscripts t and r represent the transmission and reflection, respectively, and subscript B represents the backward direction. Each supercell covers a phase range of 2π with phase differences of $\Delta\varphi_{t(tB)} = 2\pi/m_{t(tB)}$ and $\Delta\varphi_{r(rB)} = 2\pi/m_{r(rB)}$ between adjacent unit cells ($m_{t(tB)} = M/|l^{\xi}_{t(tB)}|$ and $m_{r(rB)} = M/|l^{\xi}_{r(rB)}|$ are the number of unit cells per supercell). Thus, the corresponding TRI PGM can provide transmitted and reflected intrinsic topological charges of $l^{\xi}_{t} = M\Delta\varphi_t/2\pi$ ($l^{\xi}_{tB} = -M\Delta\varphi_t/2\pi$) and $l^{\xi}_{r} = M\Delta\varphi_r/2\pi$ ($l^{\xi}_{rB} = -M\Delta\varphi_{rB}/2\pi$) for forward (backward) incidence. Because of reciprocity constraints, the transmission phase differences remain identical for both forward and backward incidences, i.e., $\Delta\varphi_t = \Delta\varphi_{tB}$, $m_t = m_{tB}$. Mirror symmetry is imposed on transmission phase twists with $l^{\xi}_{t} = -l^{\xi}_{tB}$. However, the reflection phase differences can still be different for opposite incidences [24], i.e., $\Delta\varphi_r \neq \Delta\varphi_{rB}$, resulting in $l^{\xi}_{r} \neq -l^{\xi}_{rB}$.

The acoustic waves propagating within the waveguide can generate vortex beams exhibiting Bessel-like profiles [4]. The vortex modes are determined by the working frequency and waveguide radius, which restrict the topological charge to $[-l_M, l_M]$ [18,19]. Here, l_M represents the maximum topological charge, and "+" ("−") defines clockwise (counterclockwise) helicity of phase twists observed along the propagation direction. Figure 1(d) schematically illustrates a sketch map depicting wave propagation in unit cells for opposite incidences. When the incident vortex with a topological charge of l^{f}_{i} (l^{b}_{i}) satisfies $|l^{f}_{i} + l^{\xi}_{t}| < l_M$ and $|l^{f}_{i} + l^{\xi}_{r}| < l_M$ ($|l^{b}_{i} - l^{\xi}_{t}| < l_M$ and $|l^{b}_{i} + l^{\xi}_{rB}| < l_M$), part of the wave propagating in PGM will directly transmit with T_a, while the remaining part will be immediately reflected with R_a. Here, T_a and R_a represent the averaged transmissivity and reflectivity of all unit cells, respectively. The propagation numbers of transmitted and reflected waves traveling in the PGM are defined as $L_t = 1$ ($L_{tB} = L_t$) and $L_r = 1$ ($L_{rB} = 1$), respectively [see the left in Fig. 1(d)]. The PGM can directly twist both transmitted and reflected waves and provide intrinsic topological charges, denoted by $l^{f}_{t} = l^{f}_{i} + l^{\xi}_{t}$ and $-l^{b}_{r} = l^{f}_{i} + l^{\xi}_{r}$ ($l^{b}_{t} = l^{b}_{i} - l^{\xi}_{t}$ and $-l^{f}_{r} = l^{b}_{i} + l^{\xi}_{rB}$) for forward (backward) incidence. Since the incident vortex and the reflected vortex propagate in the opposite direction, the "−" sign is added in the formula "l^{b}_{r}" or "l^{f}_{r}."

Nevertheless, when the topological charges of the emergent vortices exceed the critical value, the wave vector will become imaginary along the z direction. Consequently, direct transmission and reflection of these waves from the PGM are rendered impossible. Both transmitted and reflected waves propagating in the PGM will be internally reflected at the interface and undergo MIRs with $L > 1$. We define the normal process as the transmitted and reflected waves independently experiencing MIRs and propagating along their original paths in PGM, while the coupled process is that they are coupled to each other. In the normal process, the transmitted or reflected waves propagating within the PGM undergo a pure L_t or $L_{r(rB)}$ single trip, resulting in equivalent phase differences of $\Delta\phi = L_t\Delta\varphi_t - 2\pi q$ or $\Delta\phi = L_{r(rB)}\Delta\varphi_{r(rB)} - 2\pi q$ between adjacent unit cells, where q is an integer. The equivalent topological charge provided by the PGM is $l^D = M\Delta\phi/2\pi$ with $|l^D| < M/2$, which is calculated for the forward direction and will result in $-l^D$ for the backward direction. If the topological charge of the emergent vortex is below the maximum order l_M, i.e., $|l_i^f + l^D| < l_M$ ($|l_i^b - l^D| < l_M$), the incident vortex will attach the equivalent topological charge l^D and depart from the PGM; otherwise, the wave will experience the next internal reflection and so forth [16,18]. The scenario of $L_t = L_{r(rB)} = 2$ for both forward and backward incidences is shown in the middle in Fig. 1(d).

Since the TRI PGM possesses both transmission and reflection responses originating from nonzero T_a and R_a, the wave will not only transmit, but also be reflected during internal reflection. The coupled process occurs concurrently with the normal process. Consider the coupled processes with a total propagation number of $L = 2$ as examples [see the right in Fig. 1(d)]. For forward incidence, there are two different coupled processes shown as I and II. In process I, the reflected vortex with $|l_i^f + l_r^\xi| > l_M$ is prohibited and undergoes a secondary propagation ($L = 2$). Part of the wave transmits and experiences a subsequent $L_t = 1$ single trip (see orange arrows) instead of following the original path. The total propagation process $L = 2$ consisting of $L_r = 1$ and $L_t = 1$ provides an equivalent phase difference of $\Delta\phi = \Delta\varphi_t + \Delta\varphi_r$. In process II, the transmitted vortex cannot directly exit because $|l_i^f + l_t^\xi| > l_M$. Instead, part of the wave is reflected and undergoes the $L_{rB} = 1$ process (see black arrows). The total propagation process includes $L_t = 1$ and $L_{rB} = 1$, resulting in an equivalent phase difference of $\Delta\phi = \Delta\varphi_t + \Delta\varphi_{rB}$. In analogy, the coupled processes for backward incidence can be understood as the equivalent phase difference of $\Delta\phi = \Delta\varphi_t + \Delta\varphi_r$ in III and $\Delta\phi = \Delta\varphi_t + \Delta\varphi_{rB}$ in IV. When the emergent vortices are below the maximum order after experiencing these four coupled processes ($L = 2$), they will eventually exit. Thus, the equivalent topological charges of $l^D = M(\Delta\varphi_t + \Delta\varphi_r)/2\pi = l_t^\xi + l_r^\xi - Mq$ or $l^D = M(\Delta\varphi_t + \Delta\varphi_{rB})/2\pi = l_t^\xi - l_{rB}^\xi - Mq$ are provided by the PGM. An interesting result occurs, i.e., reflection phases can be superimposed on the transmission phases during the coupled processes, leading to TRPC. The transmissivity T_a and reflectivity R_a of the PGM are critical to the coupled processes, which must occur during MIRs with $L > 1$ and nonzero T_a and R_a. The strength of phase coupling can be described by the sound energy transfer efficiency; for example, the coupling strength is $T = T_aR_a$ in the four coupled processes. Although the I and III (II and IV) coupled processes appear to still yield mirror-symmetric equivalent phase twists with $\Delta\phi = \Delta\varphi_t + \Delta\varphi_r$ ($\Delta\phi = \Delta\varphi_t + \Delta\varphi_{rB}$), the conditions under which the coupled processes occur are different. The I (IV) process arises from the forbidden vortex reflection, while the II (III) process is induced by the disallowed vortex transmission. If we design $l_{r(rB)}^\xi$ and l_t^ξ to satisfy $|l_i^f + l_r^\xi| < l_M$ and $|l_i^f + l_t^\xi| > l_M$ ($|l_i^b + l_{rB}^\xi| < l_M$ and $|l_i^b - l_t^\xi| > l_M$) for forward (backward) incidence, only the II and III coupled processes will remain. This results in asymmetric equivalent transmission phase differences through $\Delta\varphi_r \neq \Delta\varphi_{rB}$, leading to equivalent transmission phase twists with broken mirror symmetry [see red dashed boxes in Fig. 1(d)]. In addition, when $|l_i^f + l_t^\xi| < l_M$ and $|l_i^b - l_t^\xi| < l_M$, part of the incident vortices will transmit for both forward and backward incidences without experiencing the II and III processes. The remaining I and IV coupled processes can also break the mirror symmetry of transmission phase twists with $|l_i^f + l_r^\xi| > l_M$ or $|l_i^b + l_{rB}^\xi| > l_M$. Thus, the TRPC provides a new paradigm to manipulate transmitted waves, while the MIRs offer a necessary platform.

More generally, for the emergent vortices traveling in the PGM with a total propagation number of $L = L_t + L_r + L_{rB}$, the equivalent phase difference between adjacent unit cells can be further concluded as

$$\Delta\phi = L_t\Delta\varphi_t + L_r\Delta\varphi_r + L_{rB}\Delta\varphi_{rB} - 2\pi q. \tag{1}$$

The corresponding equivalent topological charge is $l^D = L_t l_t^\xi + L_r l_r^\xi - L_{rB} l_{rB}^\xi - Mq$. When the wave undergoes internal reflection with an odd L_t and exits, it will eventually form a transmitted vortex with transmissivity $T = T_a^{L_t} R_a^{(L_r + L_{rB})}$. An even L_t will result in a reflected vortex with reflectivity $R = T_a^{L_t} R_a^{(L_r + L_{rB})}$. The topological charge of the transmitted vortex can be written as

$$\begin{matrix} l_t^f = l_i^f + l^D \\ l_t^b = l_i^b - l^D \end{matrix}, \qquad L_t = \text{odd}. \tag{2}$$

And the reflected one can be expressed as

$$\begin{matrix} -l_r^b = l_i^f + l^D \\ -l_r^f = l_i^b - l^D \end{matrix}, \qquad L_t = \text{even}. \tag{3}$$

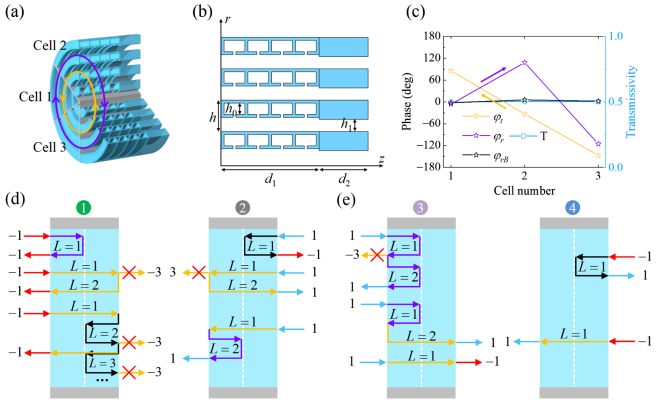

FIG. 2. Design of the TRI PGM. (a) The TRI PGM comprises of six fanlike sections with double-opening resonators and perforated panels. (b) Azimuthal part of the fanlike sections. (c) The simulated transmission and reflection phase responses and transmission spectra for each unit cell. The corresponding wave propagation process of topological charge conversion for two pairs mirror-symmetric incidences are shown in (d) and (e), respectively.

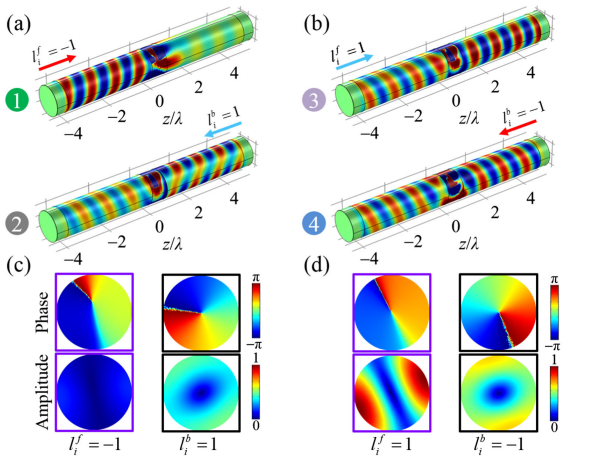

FIG. 3. Simulations of asymmetric vortex generation via PGM. (a), (b) The simulated scattered pressure fields for two pairs of mirror-symmetric incident vortices with the PGM placed at $z = 0$. (c), (d) The simulated transmission phase and amplitude distributions of total pressure field patterns at $z = -2.6\lambda$ and $z = 3.35\lambda$, respectively. The amplitudes are normalized by their maximum values.

To verify the theoretical analysis mentioned above and achieve distinct transmission phase twists, we designed a waveguide with a radius of $R = 0.64\lambda$ ($\lambda = 10$ cm), whose maximum topological charge is $l_M = 2$. The designed TRI PGM comprises six fanlike unit cells ($M = 6$), which are divided into two supercells with an angular width of $\theta_t = \theta_r = 180°$. Each supercell contains three unit cells [see Fig. 2(a)]. The phase differences between adjacent unit cells are taken as $\Delta\varphi_t = -2\pi/3$, $\Delta\varphi_r = 2\pi/3$, and $\Delta\varphi_{rB} = 0$ with intrinsic topological charges of $l_t^\xi = -2$, $l_r^\xi = 2$, and $l_{rB}^\xi = 0$. Each unit cell is constructed by rotating its azimuthal section [see Fig. 2(b)] along the z axis. The azimuthal section consists of four rows along the radius, with each row comprising four cavities and a perforated panel to stabilize transmissivity [25]. Figure 2(c) displays the simulated phase response and transmissivity of each unit cell. The transmissivities are all close to 0.5, resulting in $T_a = R_a = 0.5$. The purple and orange arrows indicate the phase twists with opposite helicity via $\Delta\varphi_r$ and $\Delta\varphi_t$, respectively. The detailed design schemes including the TRPC mechanism, constitutive relation between phases, perforated panel design, and simulation methods, are shown in Supplemental Material, Secs. A–D [21].

Considering that mirror-symmetric sound vortices of $l_i^f = -1$ and $l_i^b = 1$ are incident on the PGM from the forward and backward directions, as shown by ① and ② procedures in Fig. 2(d), one-way transmission of vortices can be achieved. The total transmissivity is $T = 0$ for forward incidence ($l_i^f = -1$) and $T = 0.25$ for backward incidence ($l_i^b = 1$), as shown in Fig. 1(a). Moreover, for another pair of mirror-symmetric incident vortices with $l_i^f = 1$ and $l_i^b = -1$, as shown by ③ and ④ procedures in Fig. 2(e), vortex transmission with different topological charges can be achieved. The transmitted vortices are composed of $l_t^f = 1$, $T = 0.25$ and $l_t^f = -1$, $T = 0.5$ for forward incidence, while the transmitted vortex is $l_t^b = 1$ and $T = 0.5$ for backward incidence, as illustrated in Fig. 1(b). The detailed topological charge conversions are provided in Supplemental Material, Sec. E [21]. Unlike the traditional way that provides only fixed phase twist, our proposed mechanism offers an extraordinary understanding of asymmetric phase generation through phase coupling. It further exhibits great potential in asymmetry, multichannel, and multifunctionality.

The simulated scattered pressure fields of the single PGM are depicted in Figs. 3(a) and 3(b), corresponding to incident vortices with $l_i^f = \pm 1$ and $l_i^b = \pm 1$, respectively. As observed, the PGM provides disparate transmission phase twists, which is clearly demonstrated by the asymmetric vortex transmission. The asymmetric transmission and reflection of mirror-symmetric incident vortices are all well presented, where the transmissivities of ①, ②, ③, and ④ procedures are 0.013, 0.215, 0.605, and 0.404 at 3430 Hz, respectively (Supplemental Material, Sec. F [21]). These simulated results are consistent with theoretical predictions, validating the presented TRPC mechanism. Cross sections of the transmitted vortex's total acoustic field patterns for forward and backward incidences are depicted in Figs. 3(c) and 3(d), respectively. The design principle is generalizable to other metasurfaces, such as coiling-up space structures [3,19], as long as they can provide the required phase responses and transmissivity. Vortex transmission with broken mirror symmetry via fanlike coiling-up space structures is also demonstrated in Supplemental Material, Sec. G [21].

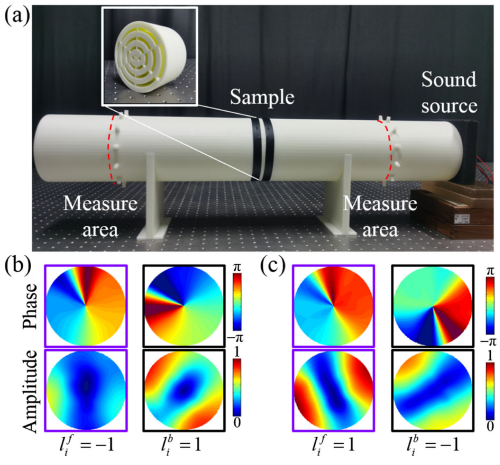

FIG. 4. Experimental demonstrations. (a) Cylindrical waveguide employed for experimental studies, with measurement areas indicated by red dashed lines. (b), (c) The experimentally measured phase and amplitude distributions of total pressure field patterns for transmission. The measured amplitudes are also normalized by the maximum values.

To confirm the broken mirror symmetry of vortex propagation, we conducted experimental validation using 3D printed samples [see Fig. 4(a)]. The total acoustic field distributions of the transmitted waves were scanned with an angular width of 30° and a step of 2.0 cm at the same position as in the simulations, as shown in Figs. 4(b) and 4(c). Despite some fabrication errors and incomplete elimination of reflections from the source, the experimental results are in good agreement with simulations. These results demonstrate that the single passive PGM can break the mirror symmetry of vortex transmission and reflection. This confirms theoretical predictions and provides valuable insights for implementing the TRPC. The details of experiment are shown in Supplemental Material, Sec. H [21].

In summary, we have presented an approach for integrated modulation of both transmission and reflection responses in a passive acoustic system. By introducing the TRPC mechanism into MIRs, we have both theoretically and experimentally demonstrated the broken mirror symmetry of vortex transmission through a single passive PGM with tailored asymmetric reflection phase responses. Compared with complicated nonreciprocal modulations [26–28], our proposed mechanism endows a single metasurface with the inherent capability to alter phase properties passively through phase modulation. This mechanism paves a flexible avenue for generating asymmetric transmission phases and enabling direction-dependent phase twists. This advancement can promote the exploration of acoustic OAM and facilitate the miniaturization and simplification of multifunctional passive OAM-based devices. Our Letter provides insight into fundamental wave physics and offers a new paradigm for asymmetric phase regulation in waveguides, especially beneficial for scalar sound lacking polarization.

This work was supported by the National Key Research and Development Program of China (2022YFA1404501 and 2021YFA1400601), the National Natural Science Fund for Distinguished Young Scholars (11925403), and the National Natural Science Foundation of China (12122406, 12192253, 12004198, and 12304486).

*Corresponding author: hcheng@nankai.edu.cn
†Corresponding author: schen@nankai.edu.cn

[1] Y. J. Shen, X. J. Wang, Z. W. Xie, C. J. Min, X. Fu, Q. Liu, M. L. Gong, and X. C. Yuan, Optical vortices 30 Years on: OAM manipulation from topological charge to multiple singularities, Light **8**, 90 (2019).
[2] Y. J. Qi, H. L. He, and M. Xiao, Manipulation of acoustic vortex with topological dislocation states, Appl. Phys. Lett. **120**, 212202 (2022).
[3] Y. R. Jia, W. Q. Ji, D. J. Wu, and X. J. Liu, Metasurface-enabled airborne fractional acoustic vortex emitter, Appl. Phys. Lett. **113**, 173502 (2018).
[4] X. Jiang, Y. Li, B. Liang, J. C. Cheng, and L. K. Zhang, Convert acoustic resonances to orbital angular momentum, Phys. Rev. Lett. **117**, 034301 (2016).
[5] L. P. Ye, C. Y. Qiu, J. Y. Lu, K. Tang, H. Jia, M. Z. Ke, S. S. Peng, and Z. Y. Liu, Making sound vortices by metasurfaces, AIP Adv. **6**, 085007 (2016).
[6] X. Jiang, B. Liang, J. C. Cheng, and C. W. Qiu, Twisted acoustics: Metasurface-enabled multiplexing and demultiplexing, Adv. Mater. **30**, 1800257 (2018).
[7] C. Z. Shi, M. Dubois, Y. Wang, and X. Zhang, High-speed acoustic communication by multiplexing orbital angular momentum, Proc. Natl. Acad. Sci. U.S.A. **114**, 7250 (2017).
[8] C. X. Zhang, X. Jiang, J. J. He, Y. Li, and D. Ta, Spatio-temporal acoustic communication by a single sensor via rotational Doppler effect, Adv. Sci. **10**, 2206619 (2023).
[9] N. Bozinovic, Y. Yue, Y. X. Ren, M. Tur, P. Kristensen, H. Huang, A. E. Willner, and S. Ramachandran, Terabit-scale orbital angular momentum mode division multiplexing in fibers, Science **340**, 1545 (2013).
[10] C. R. P. Courtney, C. E. M. Demore, H. X. Wu, A. Grinenko, P. D. Wilcox, S. Cochran, and B. W. Drinkwater, Independent trapping and manipulation of microparticles using dexterous acoustic tweezers, Appl. Phys. Lett. **104**, 154103 (2014).
[11] Z. Y. Hong, J. Zhang, and B. W. Drinkwater, Observation of orbital angular momentum transfer from Bessel-shaped acoustic vortices to diphasic liquid-microparticle mixtures, Phys. Rev. Lett. **114**, 214301 (2015).
[12] B. S. Yao, X. F. Zang, Z. Li, L. Chen, J. Y. Xie, Y. M. Zhu, and S. L. Zhuang, Dual-layered metasurfaces for asymmetric focusing, Photonics Res. **8**, 830 (2020).
[13] K. Chen, G. W. Ding, G. W. Hu, Z. W. Jin, J. M. Zhao, Y. J. Feng, T. Jiang, A. Alu, and C. W. Qiu, Directional Janus metasurface, Adv. Mater. **32**, 1906352 (2020).
[14] Y. Li, C. Shen, Y. B. Xie, J. F. Li, W. Q. Wang, S. A. Cummer, and Y. Jing, Tunable asymmetric transmission via Lossy acoustic metasurfaces, Phys. Rev. Lett. **119**, 035501 (2017).

[15] C. Shen and S. A. Cummer, Harnessing multiple internal reflections to design highly absorptive acoustic metasurfaces, Phys. Rev. Appl. **9**, 054009 (2018).
[16] Y. Y. Fu, C. Shen, Y. Y. Cao, L. Gao, H. Y. Chen, C. T. Chan, S. A. Cummer, and Y. D. Xu, Reversal of transmission and reflection based on acoustic metagratings with integer parity design, Nat. Commun. **10**, 2326 (2019).
[17] W. Q. Wang, Y. B. Xie, B. I. Popa, and S. A. Cummer, Subwavelength diffractive acoustics and wavefront manipulation with a reflective acoustic metasurface, J. Appl. Phys. **120**, 195103 (2016).
[18] Y. Y. Fu, C. Shen, X. H. Zhu, J. F. Li, Y. W. Liu, S. A. Cummer, and Y. D. Xu, Sound vortex diffraction via topological charge in phase gradient metagratings, Sci. Adv. **6**, eaba9876 (2020).
[19] Y. Y. Fu, Y. Tian, X. Li, S. L. Yang, Y. W. Liu, Y. D. Xu, and M. H. Lu, Asymmetric generation of acoustic vortex using dual-layer metasurfaces, Phys. Rev. Lett. **128**, 104501 (2022).
[20] Y. Y. Fu, Y. Y. Cao, and Y. D. Xu, Multifunctional reflection in acoustic metagratings with simplified design, Appl. Phys. Lett. **114**, 053502 (2019).
[21] See Supplemental Material at http://link.aps.org/supplemental/10.1103/PhysRevLett.132.177001 for details of limitation of traditional phase gradient metasurface, simulations, design methods, discussions of other type of metasurface, and details on the experiment, which includes Ref. [22].
[22] S. Y. Zuo, Y. Tian, Q. Wei, Y. Cheng, and X. J. Liu, Acoustic analog computing based on a reflective metasurface with decoupled modulation of phase and amplitude, J. Appl. Phys. **123**, 091704 (2018).
[23] Y. G. Tang, Y. Zhang, B. Y. Xie, H. Cheng, J. G. Tian, and S. Q. Chen, Transmission-reflection-integrated multifunctional continuously tunable metasurfaces for decoupled modulation of acoustic waves, Phys. Rev. Appl. **17**, 044027 (2022).
[24] J. F. Li, C. Shen, A. Diaz-Rubio, S. A. Tretyakov, and S. A. Cummer, Systematic design and experimental demonstration of bianisotropic metasurfaces for scattering-free manipulation of acoustic wavefronts, Nat. Commun. **9**, 1342 (2018).
[25] Y. Tian, Q. Wei, Y. Cheng, and X. J. Liu, Acoustic holography based on composite metasurface with decoupled modulation of phase and amplitude, Appl. Phys. Lett. **110**, 191901 (2017).
[26] C. P. Wiederhold, D. L. Sounas, and A. Alu, Nonreciprocal acoustic propagation and leaky-wave radiation in a waveguide with flow, J. Acoust. Soc. Am. **146**, 802 (2019).
[27] Y. F. Zhu, L. Y. Cao, A. Merkel, S. W. Fan, B. Vincent, and B. Assouar, Janus acoustic metascreen with nonreciprocal and reconfigurable phase modulations, Nat. Commun. **12**, 7089 (2021).
[28] Q. S. Wang, Z. L. Zhou, D. M. Liu, H. Ding, M. Gu, and Y. Li, Acoustic topological beam nonreciprocity via the rotational Doppler effect, Sci. Adv. **8**, eabq4451 (2022).